COMPDYN 2015
5th ECCOMAS Thematic Conference on
Computational Methods in Structural Dynamics and Earthquake Engineering
M. Papadrakakis, V. Papadopoulos, V. Plevris (eds.)
Crete Island, Greece, 25–27 May 2015

SEISMIC EVALUATION OF EMBANKMENT-TYPE STRUCTURES WITH COUPLED HYDRO-MECHANICAL MODEL

I. Rapti[1,2], F. Lopez-Caballero[1], A. Modaressi-Farahmand-Razavi[1], A. Foucault[2], F. Voldoire[2]

[1]Laboratoire MSS-Mat CNRS UMR 8579, Ecole Centrale Paris
Grande Voie des Vignes 92295, Châtenay-Malabry Cedex, FRANCE
e-mail: {ioanna.rapti,fernando.lopez-caballero,arezou.modaressi}@ecp.fr

[2]Institut des Sciences de la Mécanique et Applications Industrielles, EDF-CNRS-CEA-ENSTA UMR 9219
1 Avenue du Général de Gaulle, 92140 Clamart, FRANCE
e-mail: {alexandre.foucault,francois.voldoire}@edf.fr

Keywords: Embankment, Dynamic analysis, Coupled hydro-mechanical model, Liquefaction.

Abstract. *The response of geotechnical structures under earthquake loading is highly nonlinear and often leads to problems of slope stability, foundation settlement and soil liquefaction. The prediction of these failure modes is a topic of great interest in geotechnical earthquake engineering, particularly for structural integrity assessment, which requires estimation of structural behavior during and after collapse. In this study, the earthquake response of a road embankment resting on a soil foundation is investigated. Both fully drained and coupled effective stress analysis are performed. Moreover, two different soil types are used for the embankment (loose-to-medium and medium-to-dense sand). In the fully drained case, no failure of the embankment is observed for the medium-to-dense sand and for a certain level of ground motion. However, in the coupled effective stress simulation, for the same material and input motion, liquefaction of the foundation soil can lead to the generation of a thick shear band which produce large settlements and accelerate the failure of the embankment. The response of the loose-to-medium sand is fundamentally different, as several localization zones are generated, at the foundation part and inside the embankment body, as well. In both simulations - fully drained and coupled effective stress analyis - the embankment fail can occur due to shear band generation inside the embankment.*

1 INTRODUCTION

Localization phenomena are observed in most structural failures and can cause huge material and human damage. Localization phenomena have proven particularly challenging to model in conventional finite-element simulations. Several studies have analyzed earthquake triggered landslides and the effect of ground-shaking on dry foundation-structure systems founded near slope crests with a strain-softening soil [1]. The apparition of a shear band extending from toe to crest was identified as failure mode, as soil has reached or exceeded its peak shear strength. The fact that mesh dependency phenomena may appear was also taken into account and explored through a parametric dynamic analysis. After a dynamic parametric analysis of a road embankment subjected to various amplitude ground motions, no significant mesh dependency is observed in dry conditions and the localization zone initiates from the toe, due to the geometric anomaly and produces the failure of the embankment [2].

A road embankment resting on liquefiable soil and subjected to the 2011 Off the Pacific Coast of Tohoku earthquake is simulated by [3]. Their results showed that when the water-saturated region in the embankment liquefies, it leads to large settlements and inclined shear localization zones inside the embankment body.

In this study, the earthquake response of a road embankment resting on a soil foundation is investigated. A plane-strain finite element model is built to analyze the arising failure modes and earthquake induced deformations. Two different materials are used for the embankment, a loose-to-medium and medium-to-dense sand. Moreover, fully drained and coupled effective stress analysis are simulated for both materials. Modeling of advanced soil behavior is achieved using the fully coupled effective stress ECP constitutive model developed at *Ecole Centrale Paris* [4]. Numerical simulations are performed using the open-source FE software Code_Aster, developed by EDF.

In the first section, the numerical model is presented. Thereafter, the dynamic analysis of the road embankment is presented for both materials and simulations. The effect of liquefaction on the foundation of the embankment is evaluated with the coupled hydro-mechanical analysis.

2 NUMERICAL MODEL

2.1 Geometry - Boundary conditions

Two different models are used for the purpose of this study. A thin elastic layer of 0.25m is placed at the top of the embankment, representing a pavement layer. In the first model, the dry road embankment is composed of a medium-to-dense sand (MDS), while in the second one, a loose-to-medium sand (LMS) is used. In both cases, it is placed over a loose-to-medium contractive saturated sand (LMS) substratum and the water table is situated 1m below the embankment. At the lower part of the foundation a dense saturated sand is used. The embankment's slope inclination is equal to 1:2 (vertical:horizontal). The dimensions of the model and its geometry are presented in Fig. 1.

Lateral horizontal displacements are fixed (u_x=0) and the substratum is founded on a rigid base. No flux is possible at the lateral surfaces and at the base. These boundary conditions are equivalent to those of a centrifuge test. The mesh consists of 6-node triangular elements of 0.25m length on average.

The model was constructed in three steps. First, a static analysis was performed in order to proceed to stress initialization. Afterwards, an excavation took place at the right upper part of the embankment. The last step was the dynamic analysis, so as to impose the input seismic signal. In all analyses gravity loading is taken into account.

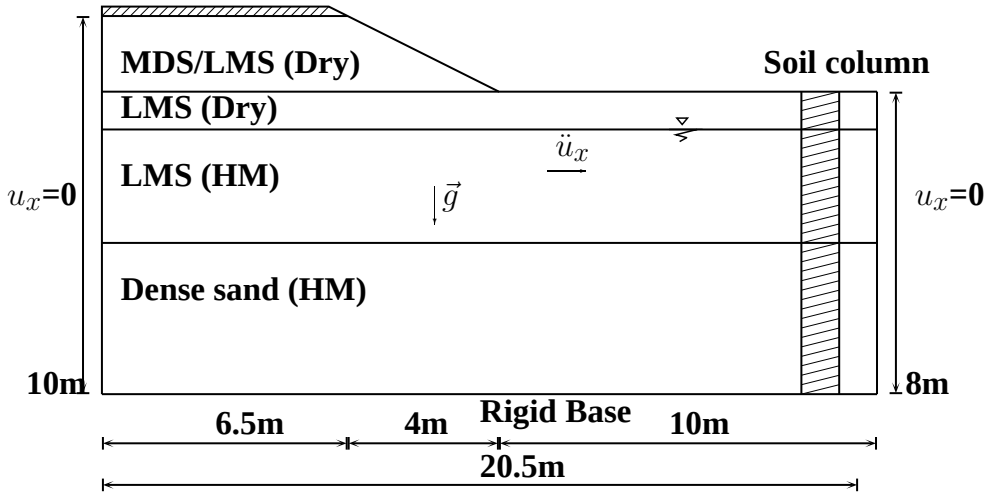

Figure 1: Illustration of numerical model.

The implicit method of Newmark integration is used for the dynamic analysis. Numerical damping equal to ξ = 0.2% is added to the model, as the set of integration parameters used is β = 0.31 and γ = 0.61 [5, 6]. Since, the model is elastoplastic, no damping exists in the elastic domain and numerical damping should be added.

2.2 Mechanical characteristics

The ECP elastoplastic multi-mechanism model [4] is used to represent soil behavior under cyclic loading. This model can take into account soil behavior in a large range of loading paths. The representation of all irreversible phenomena is idealized by four coupled elementary plastic mechanisms: three plane-strain deviatoric plastic deformation mechanisms in three orthogonal planes and an isotropic one. The model uses a Coulomb-type failure criterion and the critical state concept. The evolution of hardening is based on plastic strain (deviatoric and volumetric strain for the deviatoric mechanisms and volumetric strain for the isotropic one). To take into account cyclic behavior both isotropic and kinematical hardenings are used. An implicit integration scheme is used for the equations of the model [7]. The model takes into account non-linear elasticity. Elastic mechanical characteristics E, ν must also be defined.

Adopting the soil mechanics sign convention (compression positive), the deviatoric primary yield surface of the k plane is given by:

$$f_k(\sigma', \varepsilon_v^p, r_k) \quad = \quad q_k - sin\phi'_{pp} \cdot p'_k \cdot F_k \cdot r_k \tag{1}$$

where p'_k and q_k are the effective mean and deviatoric values of stress tensors, ϕ'_{pp} is the friction angle at critical state, the function F_k permits to control the isotropic hardening associated with the plastic volumetric strain, whereas r_k accounts for the isotropic hardening generated by plastic shearing. They represent progressive friction mobilization in the soil and their product reaches unity at perfect plasticity.

In Fig. 2, the curves of deviatoric stress - deviatoric deformation (q-ε_d) are plotted for all materials, after drained and undrained triaxial test simulations. All triaxial tests were carried out at confining pressures corresponding to the average geostatic pressure of each layer, i.e. 17kPa and 45kPa for the dry medium-to-dense and loose-to-medium sand (see Fig.2a), and 60kPa and

90kPa for the saturated loose-to-medium and dense sand (see Fig.2b,2c), respectively. Material parameters can be found in Table 1.

Table 1: ECP model's parameters for the soil.

Parameter	MDS (Embankment)	LMS (Embankment/Foundation)	Dense sand (Foundation)
ρ [kg/m^3]	1755	1755	1755
ν [·]	0.3	0.3	0.4
K_0 [·]	0.5	0.7	0.7
Elasticity			
E [MPa]	571.65	754	1850
n_e [·]	0.4	0.5	0.47
p_{ref} [MPa]	1.0	1.0	1.0
Critical State and Plasticity			
β [·]	43	33	44
b [·]	0.2	0.12	0.8
d [·]	3.5	2.0	5.0
ϕ [^{o}]	31	30	37
p_{c0} [MPa]	1.8	$40{\cdot}10^{-3}$	0.4
Flow Rule and Hardening			
a_{mon} [·]	0.004	0.005	0.0004
a_{cyc} [·]	0.0001	0.0001	0.0002
c_{mon} [·]	0.06	0.004	0.01
c_{cyc} [·]	0.03	0.002	0.005
ψ [^{o}]	31	30	37
α [·]	1.0	1.0	1.0
χ_m [·]	1.0	1.5	1.0
Threshold Domains			
r^d_{ela} [·]	0.005	0.03	0.005
r^{iso}_{ela} [·]	0.001	0.001	0.0001
r^d_{cyc} [·]	0.005	0.03	0.005
r^{iso}_{cyc} [·]	0.001	0.001	0.0001
r_{hys} [·]	0.03	0.04	0.04
r_{mob} [·]	0.8	0.8	0.8

2.3 Hydraulic parameters

Two different simulations are performed, in order to evaluate the effect of the pore water pressure generation, one fully drained and one coupled effective stress analysis [8]. In Table 2, the hydraulic parameters of each material are presented.

2.4 Input motions

In order to test the dynamic response of the model, a nonlinear soil column with similar material profile was subjected to 6 ground motions chosen from the Pacific Earthquake Engineering Research Center (PEER) database and a coupled effective stress analysis was performed.

The peak ground acceleration (PGA) in free field was calculated as function of the maximum acceleration of the input signal ($a_{bed,max}$) for all ground motions (Fig. 3). Soil liquefaction was observed for moderate and strong input ground motions with $a_{bed,max}$ >0.2g.

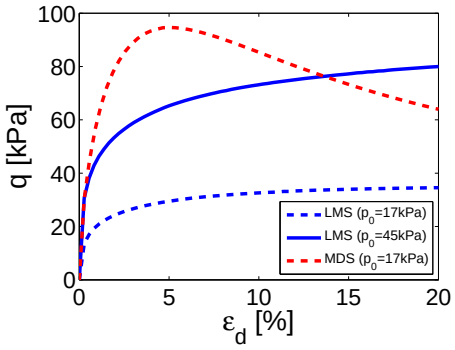

(a) Triaxial drained test (MDS / LMS).

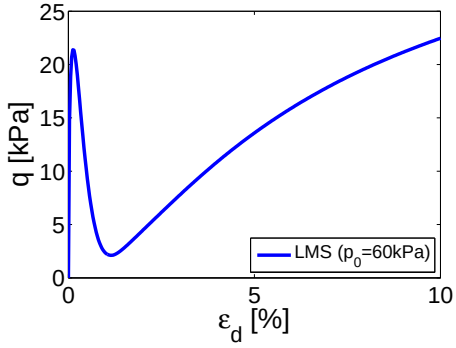

(b) Triaxial undrained test (LMS).

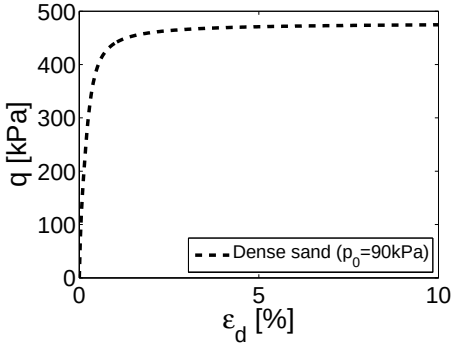

(c) Triaxial undrained test (Dense sand).

Figure 2: Soil response of one material point - ECP constitutive model: q-ε_d.

Table 2: Hydraulic parameters for the soil.

Parameter	**Foundation (LMS)**	**Foundation (Dense sand)**
Fluid mass density, ρ_w [kg/m^3]	1000	1000
Porosity, n [·]	0.35	0.35
Water dynamic viscosity, μ_w [kg/m·s]	0.001	0.001
Permeability, k_s [m/s]	$1{\cdot}10^{-4}$	$1{\cdot}10^{-5}$
Fluid compressibility, H_w [Pa^{-1}]	$3.3{\cdot}10^{-8}$	$3.3{\cdot}10^{-8}$

Consequent to these results and in order to evaluate the response of the embankment due to the liquefiable foundation, a moderate motion ($a_{bed,max}$=0.24g) is used as input signal (see accelerogram and Arias intensity of input motion in Fig.4).

3 DYNAMIC ANALYSIS OF ROAD EMBANKMENT

In this section the results of the dynamic response of the road embankment subjected to the input motion of Fig.4 are presented, for both fully drained and coupled effective stress analysis and for both materials used at the part of the embankment (MDS/LMS). In the first simulation, effective stresses and zero pore water pressure are considered, while in the coupled simulation, the pore water pressure is taken into account [8]. Both simulations start from the same effective stress state at the beginning of the dynamic analysis, as shown in Fig. 5 for the LMS.

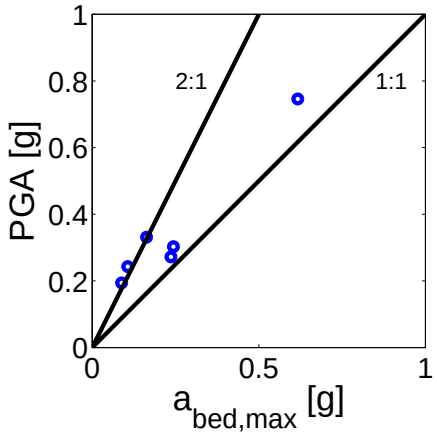

Figure 3: PGA - $a_{bed,max}$ for the soil column.

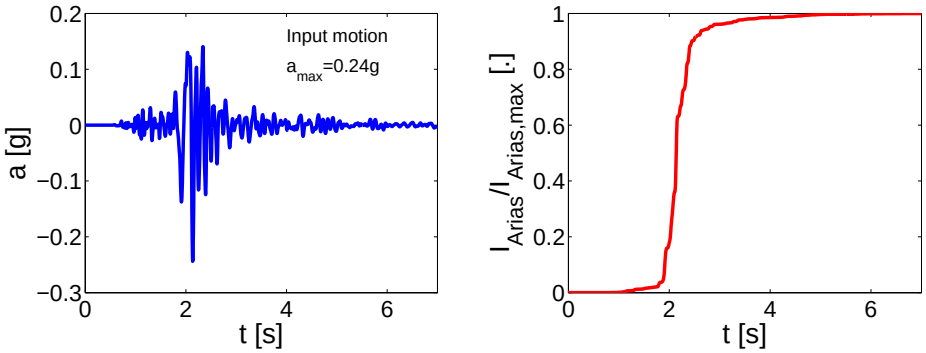

(a) Accelerogram. (b) I_{Arias} intensity.

Figure 4: Input moderate seismic signal.

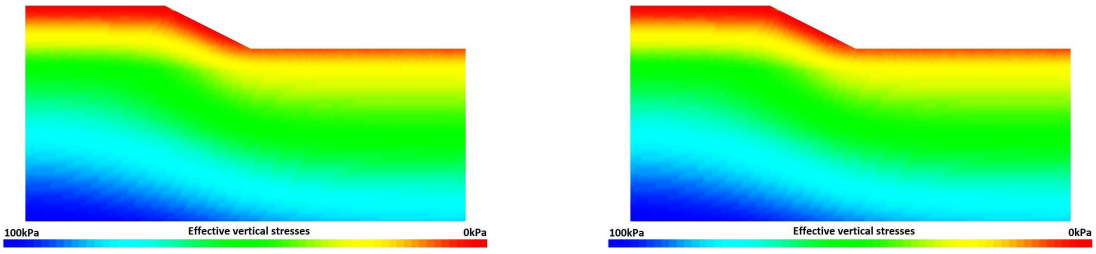

(a) Fully drained effective stress simulation. (b) Coupled effective stress simulation.

Figure 5: Initial vertical effective stresses $\sigma'_{v,0}$ for both simulations (LMS).

3.1 Fully drained effective stress simulation

In the fully drained approach, the embankment with the MDS stays almost unaffected by the ground motion, while in the model with the LMS, greater displacements are observed close to the slope. Particularly, in Fig.6 the deformed shape of horizontal and vertical displacements at the end of the motion are plotted. Horizontal displacement ($\simeq$2cm) is detected close to the slope and settlement at the upper part of the embankment.

Subsequently, the stability of the embankment is tested by calculating the second order work

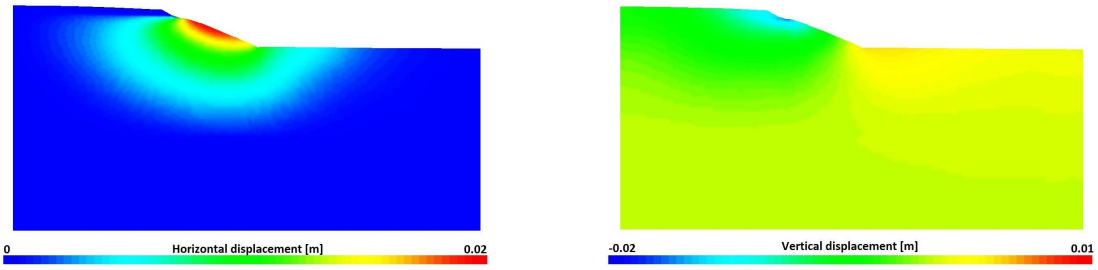

(a) Horizontal displacement. (b) Vertical displacement.

Figure 6: Deformed shape at the end of the ground motion (Fully drained effective stress simulation - LMS).

($d^2W=\dot{\sigma}:\dot{\varepsilon}$) [9, 10]. In this study the second order work is calculated in terms of invariants, i.e. $d^2W=\dot{p}:\dot{\varepsilon_v}+\dot{q}:\dot{\varepsilon_d}$. During the main shock of the ground motion, the embankment - with both materials - remains stable, as $d^2W>0$ and for the sake of brevity, the figures are omitted as no important information is provided.

In the MDS model, as the embankment is very rigid no remarkable deformations appear. Only the upper part, at the interface with the elastic pavement layer, is affected and generates shear strains (see Fig.7a). However, in the case of LMS, a shear band extending from toe to crest is identified (Fig.7b). A stronger input motion will increase the level of deviatoric strains and the embankment can fail due to this shear band generation.

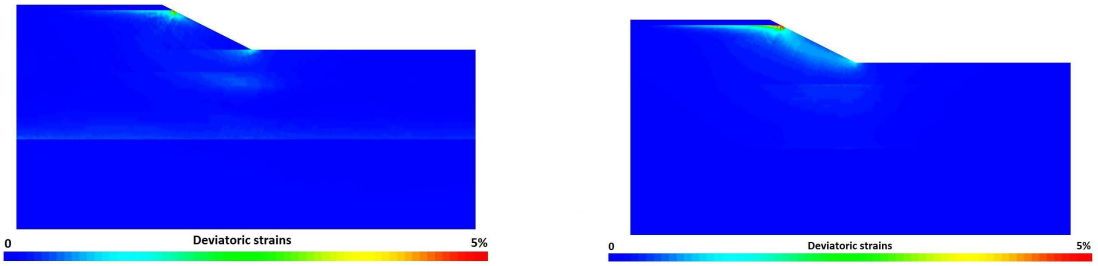

(a) MDS (b) LMS

Figure 7: Deviatoric strains ε_d at the end of the ground motion (Fully drained effective stress simulation).

3.2 Coupled effective stress simulation

In the case of coupled effective stress simulation, the effect of excess pore water pressure in the foundation part is significant for both materials. The liquefied soil at the foundation creates an extended failure zone. In both models (MDS/LMS) almost the whole part of the embankment settles and moves to the right, as a large part of the foundation moves to the right, too, and swells due to the excess pore water pressure. More important displacement and settlement is remarked for the LMS model and its deformed shape at the end of the ground motion is presented in Fig.8. As the embankment is assymetric and it is constrained at the left boundary, it tends always to move to the right.

During the main shock (between 2-3s) excess pore water (Δp_w) pressure is observed in the foundation part of LMS. In Fig.9a,9b,9c, the contours of r_u ($\Delta p_w/\sigma'_{v,0}$) are plotted for the LMS

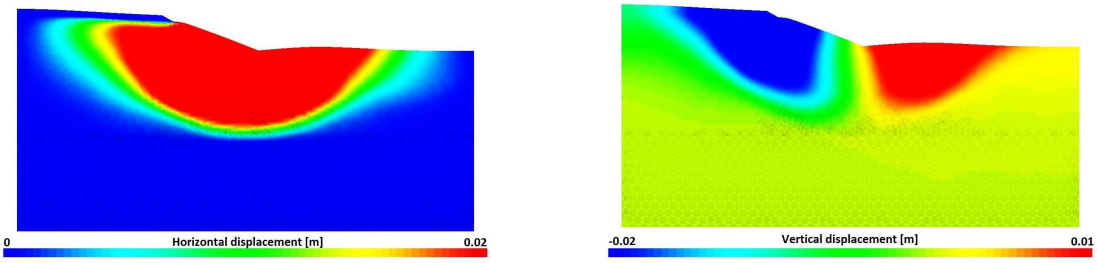

(a) Horizontal displacement. (b) Vertical displacement.

Figure 8: Deformed shape at the end of the motion (Coupled effective stress simulation - LMS).

model at various instants of the ground motion. The soil has almost liquefied in the foundation part of LMS, as $r_u \simeq 0.8$. The evolution of excess pore water pressure can be related to the Arias intensity (Fig.4b), as between t=2-3s the total intensity of the motion has been accumulated. The same response was obtained for the MDS, but the zone of liquefied soil was sligthly thinner. Progressively, the dissipation of pore water pressure starts, as the strength of the ground motion decreases (see Fig.9d for LMS).

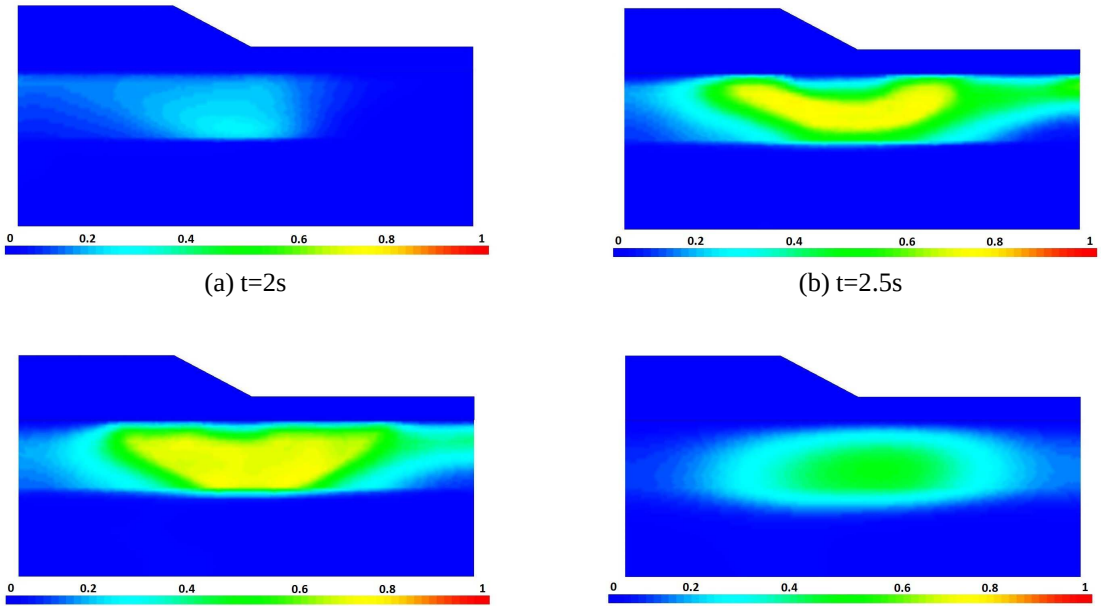

(a) t=2s (b) t=2.5s

(c) t=3s (d) t=7.4s (end)

Figure 9: Excess pore water pressure ratio during the motion (r_u) - LMS.

Concerning the stability of the embankment, during the liquefaction phase (2-3s), the embankment becomes unstable ($d^2W < 0$). A circular surface of instability appears in both models (MDS/LMS) which implies the expected failure mode (Fig.10a for MDS, Fig.10b for LMS). Note that the instability becomes more significant in the embankment with the LMS, as almost the whole embankment is unstable.

In the case of MDS model, a localization zone of shear strains is remarked in the foundation part of LMS at the end of the ground motion (see Fig.11a). This shear zone extends through the liquefied soil and leads to the circular failure mode of the foundation. Contrary to the fully

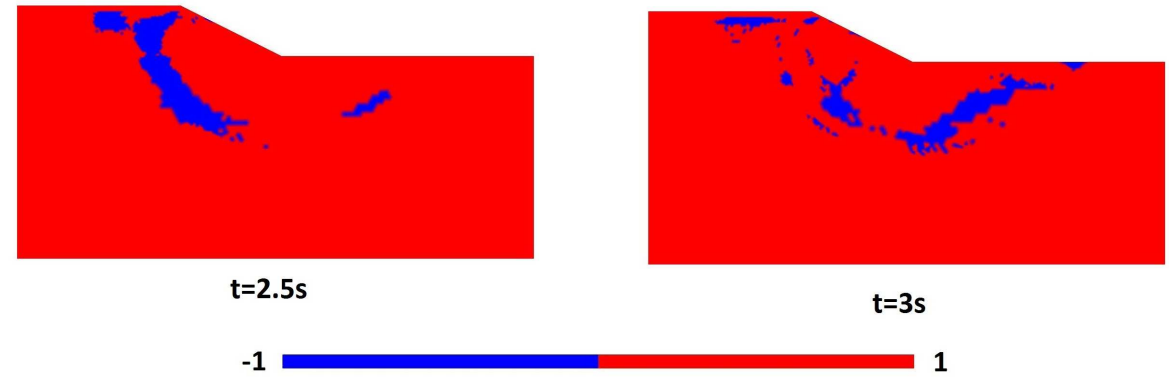

(a) MDS

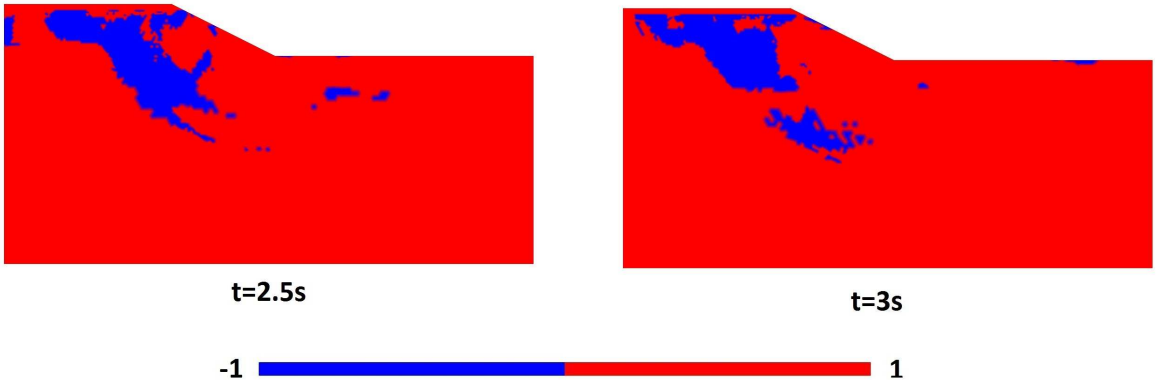

(b) LMS

Figure 10: Second order work (Coupled effective stress simulation).

drained case, where no shear strain generation is remarked (Fig.7a) and the only deformations observed are those at the interface with the elastic pavement layer.

However, in the case of LMS model, two different zones of localization of shear deformations are noticed (Fig.11b). Due to the liquefaction at the foundation part of LMS, a thick and more extended zone of shear strains appears. Moreover, a second shear band is observed inside the embankment body (see zoom of the shear band in Fig.11c), as detected previously in the fully drained approach (Fig.7b). Consequently, it should be highlighted the fact that in the case of coupled simulation with a loose material at the embankment part, two different shear zones are generated and lead to failure.

4 CONCLUSIONS

In this study, an analysis of earthquake-induced liquefaction is presented using a fully-coupled hydromechanical model. The effect of a liquefiable foundation on the failure mode of a river embankment is discussed. Two different materials are used for the embankment (MDS/LMS), so as to better investigate the failure mode.

Firstly, a fully drained effective stress approach shows that the embakment consisting of a dense-rigid material is generally unaffected by the moderate motion. Nevertheless, in the case of a loose embankment, a shear band generates from the toe and extends to the crest.

In the coupled effective stress analysis, where the pore water pressure is taken into account,

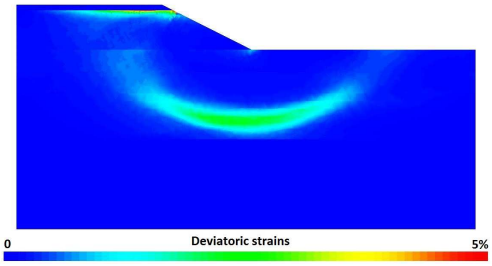

(a) MDS

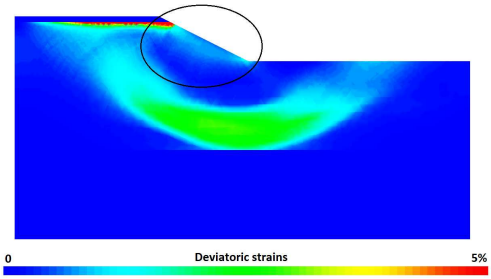

(b) LMS

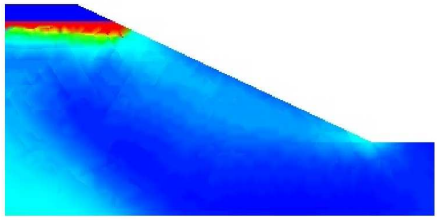

(c) Zoom of shear band (LMS).

Figure 11: Deviatoric strains ε_d at the end of the ground motion (Coupled effective stress simulation).

the embankment with both materials is strongly affected. A liquefied zone at the foundation part leads to noticeable settlement and horizontal displacement. A circular failure mode is produced and a zone of shear deformations at the liquefied foundation part is pointed out at the end of the motion. Furthermore, in the model with the loose sand, a second shear band inside the embankment body amplifies the displacements and leads to an extended failure.

To conclude, the effect of excess pore water pressure is of highly importance, as a stable embankment - in fully drained conditions - becomes unstable in coupled analysis and is leaded to failure due to a liquefiable zone in the foundation. It should also be remarked the double shear band generation in the case of the loose embankment.

In future work, dynamic analyses with stronger seismic motions should be performed, in order to reach flow liquefaction with larger settlements and total collapse. Post-liquefaction effects (settlements) should be also examined. This work can be considered as a first step for dynamic analysis of large scale structures, such as seismic response of earth dams.

REFERENCES

[1] R. Kourkoulis, I. Anastasopoulos, F. Gelagoti, and G. Gazetas, “Interaction of foundation-structure systems with seismically precarious slopes: Numerical analysis with strain softening constitutive model,” *Soil Dynamics and Earthquake Engineering*, vol. 30, pp. 1430–1445, 2010.

[2] I. Rapti, A. Foucault, and E. C. Paris, “Strain localization of a road embankment founded on soil substratum due to seismic loading,” in *9th International Conference on Structural Dynamics, EURODYN 2014. Porto, Portugal, 30 June - 2 July 2014*, vol. 1, pp. 681–688, 2014.

[3] H. Sadeghi, S. Kimoto, F. Oka, and B. Shahbodagh, "Dynamic analysis of river embankments during earthquakes using a finite deformation FE analysis method," in *14th International Conference of the International Association for Computer Methods and Advances in Geomechanics*, no. 2011, (Kyoto, Japan), pp. 637–642, 2014.

[4] J.-C. Hujeux, "Une loi de comportement pour le chargement cyclique des sols," *Presses ENPC*, pp. 278–302, 1985.

[5] S. Kontoe, L. Zdravkovic, and D. Potts, "An assessment of time integration schemes for dynamic geotechnical problems," *Computers and Geotechnics*, pp. 253–264, 2008.

[6] S. Ruiz and G. Saragoni, "Free vibration of soils during large earthquakes," *Soil Dynamics and Earthquake Engineering*, vol. 29, pp. 1–16, 2009.

[7] A. Foucault, "Loi de comportement cyclique de Hujeux pour les sols," *Documentation of Code_Aster [R7.01.23]*, 2009.

[8] S. Montoya-Noguera and F. Lopez-Caballero, "Effect of coupling excess pore pressure and deformation on nonlinear seismic soil response," *Acta Geotechnica*, 2015.

[9] R. Hill, "A general theory of uniqueness and stability in elastic-plastic solids," *Journal of Mechanics and Physics of Solids*, vol. 6, pp. 236–249, 1958.

[10] K. Hamadi, A. . Modaressi-Farahmand Razavi, and F. Darve, "Bifurcation and instability modelling by a multimechanism elasto-plastic model," *International Journal for Numerical and Analytical Methods in Geomechanics*, vol. 32, pp. 461–492, 2008.